

# Large-Signal Stability Guarantees for a Scalable DC Microgrid with Nonlinear Distributed Control: The Slow Communication Scenario

Cornelia Skaga, *Member, IEEE*, Mahdiah S. Sadabadi, *Senior Member, IEEE*, and Gilbert Bergna-Diaz, *Member, IEEE*

**Abstract**—The increasing integration of renewable energy sources into electrical grids necessitates a paradigm shift toward advanced control schemes that guarantee safe and stable operations with scalable properties. Hence, this study explores large-signal stability guarantees of a promising distributed control framework for cyber-physical DC microgrids, ensuring proportional current sharing and voltage containment within pre-specified limits. The proposed control framework adopts nonlinear nested control loops—inner/decentralized and outer/distributed—specifically designed to simultaneously achieve the control objectives. Our *scalable* stability result relies on singular perturbation theory to prove global exponential stability by imposing a sufficient time-scale separation at the border between the nested control loops. In particular, by saturating the influence of the outer loop controller in the inner loop, the proposed controller preserves a more convenient mathematical structure, facilitating the scalability of the stability proof using Lyapunov arguments. The effectiveness of our proposed control strategy is supported through time-domain simulations of a case-specific low-voltage DC microgrid following a careful tuning strategy, and a small-signal stability analysis is conducted to derive *practical guidelines* that enhance the applicability of the method.

**Index Terms**—DC microgrid, distributed control, singular perturbation theory, stability of nonlinear systems.

## I. INTRODUCTION

Modern power systems are strategically evolving into converter-dominated, multi-agent grids to enable profitable and efficient integration of distributed (renewable) energy resources (DER) such as photovoltaics, wind turbines, battery energy storage systems, and electric vehicles [1], [2]. Furthermore, the inherent electrical nature of most renewable energy sources (RES), along with modern generation and load technologies, positions multi-agent DC microgrids (MGs) as a promising solution for optimizing local power utilization of these DER, ascribed to their high flexibility and operational advantages to operate in both *grid-connected* and autonomous modes of operations (*islanded*) [3], as well as their simplified dynamics, control, and management [4]. Traditionally, power grids are controlled in a centralized manner, with a single control unit gathering data from the wide-area power grid network. Centralized frameworks often require a sparse communication network, are easy to implement, and are often able to obtain globally optimized solutions [5]. However, as the centralized controller is highly dependent on global system information, the

framework is highly susceptible to single-point-of-failure (SPoF) and communication-related disturbances such as communication delays, data-link failures, and data packet losses, while scalability also remains a challenge [5]–[7]. Hence, the control configurations of modern multi-agent grids – interconnecting an expanding number of DER – are undergoing a paradigm shift toward communication-reliant distributed control schemes to enhance flexibility, scalability, and reliability [8]–[10]. Distributed control strategies often include primary local control of the power electronic converters for local stabilization of the distributed generation units (DGs), and a secondary distributed controller– leveraging high bandwidth communication between neighboring agents to cooperatively restore initial conditions [11].

However, these converter-dominated DC grids exhibit low electrical inertia and weak damping, making them vulnerable to transient disturbances and less robust against random perturbations, underscoring the need for scalable control strategies that ensure sufficient stability guarantees [12], [13].

### A. Research Gap

From a performance perspective, this growing integration of DER introduces challenges related to precise voltage stability and power flow management [14]. As a result, proportional load sharing (current- or power sharing) among DGs, along with stable and precise voltage regulation, are typically considered as the primary control objectives in DC microgrids [7], [15]. Voltage regulation is essential for ensuring the proper operation of interconnected loads, commonly achieved by maintaining the average voltage across the MG at a global set-point value [16], and load sharing is gaining interest as it enhances scalable capabilities [17]. Conventionally, adapting hierarchical control schemes (such as secondary distributed control frameworks) facilitates the achievement of both objectives simultaneously [16]. Several distributed communication-based (cooperative) control configurations for DC MGs have been proposed in the literature [17]–[24], demonstrating the feasibility of achieving simultaneous current sharing and average voltage regulation. However, average voltage regulation may lead to significant deviations in individual generator voltages, potentially exceeding operational limits [4]. To overcome these limitations, [4] introduces a novel nonlinear distributed control framework, relying on nested control loops– inner/decentralized/primary and outer/distributed/secondary– to ensure that all energized units contribute power proportionally to their rated capacities while dynamically operating within predefined voltage limits. However, the nonlinear control framework was proposed without any guarantee of stability. Lyapunov’s direct method – commonly used in large-signal stability analysis of nonlinear systems– can indeed be used to assess the stability of the case-specific system with a defined (and preferably

The preliminary results of this paper are presented in [1].

Cornelia Skaga with the Department of Electric Energy, Norwegian University of Science and Technology (NTNU), 7491 Trondheim, Norway (e-mail: cornelia.skaga@ntnu.no).

Mahdiah S. Sadabadi is with the Department of Electrical and Electronic Engineering, The University of Manchester, M13 9PL, Manchester, UK (e-mail: mahdiah.sadabadi@manchester.ac.uk).

Gilbert Bergna-Diaz is with the Department of Electric Energy, Norwegian University of Science and Technology (NTNU), 7491 Trondheim, Norway (e-mail: gilbert.bergna@ntnu.no).

low) number of generators admitting the structure given in [4]. That being said, as the proposed control framework employs nested control loops, obtaining a scalable Lyapunov candidate of the general  $n$ -generator case becomes nontrivial, thereby limiting its scalability in practice. Moreover, to address the challenges posed by nonlinear nested control loops, [25] employs the *Popov* multiplier in conjunction with Lyapunov theory to ensure large-signal stability of a stand-alone converter. Preliminarily, the approach relies on reformulating the closed-loop system into a suitable *lure-like* representation isolating the static nonlinearity. This facilitates the derivation of dissipativity-based conditions under which Lyapunov stability can be established. Even though the result in [25] is a non-conservative large-signal stability certificate, its current formulation seems to be case-specific.

### B. Contributions

To derive a large-signal stability certificate that ensures *scalable* Plug-and-Play (PnP)-properties while addressing the nonlinear nested control loops in [4], this paper reformulates the system as a singularly perturbed problem with time-scale separation, and applies Lyapunov theory to establish Global Exponential Stability (G.E.S.). This approach is motivated by the methodology presented in [2], where an almost identical control strategy was proposed for AC grids to ensure scalable global asymptotic stability conditions. That proof relied on singular perturbation theory (SPT), accommodating scalable stability conditions under reasonable time-scale assumptions for AC grids; i.e., the distributed outer loop exhibits fast behavior while the electrical system operates at a slower time-scale. Moreover, our preliminary work in [26] extends the theoretical foundation in [2] to the DC grid in [4], guaranteeing scalable G.E.S. under similar time-scale assumptions. However, a more common practice in DC grids is arguably to operate the system with fast electrical- and inner-loop control dynamics and slower communication-based (outer-loop) control. Hence, this paper extends the results in [1] by applying singular perturbation theory to prove G.E.S. with promising scalable properties, imposing a sufficient time-scale separation between the fast electrical- and inner-loop control system and the slower communication dynamics, and thus preserving a more convenient mathematical structure for using (scalable) Lyapunov arguments [27]. To facilitate this, we implement additional modifications to the proposed distributed control strategy in [4]. In particular, *we saturate the influence of the distributed outer loop controller in the decentralized inner loop*. It is worth noting that formulating the system as a singularly perturbed stability problem includes the G.E.S. analysis of the *reduced-system*. This result alone—that is, excluding the boundary-layer and interconnection terms—can already be viewed as a more accurate stability analysis of the slow dynamics (distributed control/communication network) as it is being performed under a *quasi-static* electrical model; i.e., without fully neglecting the fast dynamics.

This paper improves our preliminary results reported in [1]. First, we update our controller in the following ways: we include a proportional term to satisfy commonly used industrial PI controllers, and implement a constant leakage function in our local regulator for improved performance. We show how the proportional controller substantially contributes to current peak shaving, particularly when combined with careful tuning of the voltage saturation. Second, the stability proof has been substantially updated and revised, accommodating these control modifications as well as establishing G.E.S. in

both saturated and unsaturated operations. Third, we update our case studies and simulation results to provide empirical validation of the theoretical assumptions and conclusions. In particular, we demonstrate that satisfactory control parameter tuning yields sufficient monotonicity conditions, which are instrumental in concluding G.E.S. in the stability proof. Finally, we complement the study with a small-signal stability analysis to reduce the conservativeness of the large-signal stability tuning conditions. In particular, this analysis provides some practical guidelines for increasing the slow communication rate required by the proof, and thus enhancing the applicability of the controller.

The rest of the paper is structured as follows. Section II presents the model of the electrical system and the proposed control framework. In Section III, we present the main result of this paper: a comprehensive stability proof for a closed-loop DC microgrid with a nonlinear distributed controller, that under certain tuning conditions can stabilize to a desired (optimal) steady-state. Furthermore, the controller is tested in Section IV via time-domain simulations on a 4-terminal DC microgrid to showcase the effectiveness of the method, followed by a small-signal stability analysis. Finally, Section V concludes this paper.

## II. SYSTEM MODELING AND CONTROL FRAMEWORK

Throughout the paper, we use the following notations:  $\mathbb{R}^{n \times m}$  and  $\mathbb{R}^n$  denote a set of  $n \times m$  real matrices and  $n \times 1$  real vectors, respectively.  $\text{col}(\dots) \in \mathbb{R}^n$  denotes a column vector and  $\text{bcol}\{\dots\} \in \mathbb{R}^n$  denotes a column vector of vectors.  $\text{diag}(\dots) \in \mathbb{R}^{n \times n}$  denotes a diagonal matrix with scalar entries, and  $\text{bdia}\{\dots\} \in \mathbb{R}^{n \times n}$  denotes a diagonal matrix of vectors. Given a scalar or a vector  $x$ , the value at the equilibrium point is indicated as  $\bar{x}$ , and  $\tilde{x}$  denotes a shifted variable where  $\tilde{x} \triangleq x - \bar{x}$ . Moreover, we use the block vector notation  $x^b$ , for any subset  $b \subseteq \mathcal{G} \cup \mathcal{E} \cup \mathcal{N}$ , where  $x^b$  denotes the vector collecting the states associated with the indices in  $b$ . Note that  $\mathcal{G} = \{1, 2, \dots, n_i\}$  is the set of distributed generators,  $\mathcal{E} = \{1, 2, \dots, n_j\}$  is the set of transmission lines, and  $\mathcal{N} = \{1, 2, \dots, n_k\}$  is the set of power consuming loads.

### A. Dynamical model of the DC Microgrids

The architecture of the DC microgrids is inherently multilayered, comprising a physical layer that interconnects agents and loads via RL-modeled transmission lines, and a cyber layer that facilitates information exchange among neighboring agents. The agents are the distributed generators (DGs), located close to the power-consuming loads (ZI-loads), and are effectively interfaced with the rest of the MG through voltage-controlled converters. The converters are considered equivalent zero-order models, hence, the internal voltage controller and associated dynamics are not considered in this paper. The DGs are interconnected both electrically and via distributed communication links, forming a cyber-physical grid. Graph theory is used to establish the physical and virtual interconnections, see Appendix A in [2] for the precise definitions of the included graphs. Following the model presented in Fig.1, the electrical dynamics for the  $i$ th DG, connected to the  $j$ th transmission line and the  $k$ th power-consuming load are presented in (1).

$$L_i^G \dot{I}_i^G = u_i - \sum_k b_{ik}^G V_k^N - R_i^G I_i^G, \quad (1a)$$

$$L_j^E \dot{I}_j^E = - \sum_k b_{jk}^E V_k^N - R_j^E I_j^E, \quad (1b)$$

$$C_k^N \dot{V}_k^N = \sum_j b_{kj}^E I_j^E + \sum_i b_{ki}^G I_i^G - G_k^{\text{cte}} V_k^N - I_k^{\text{cte}}, \quad (1c)$$

where  $L_i^G$ ,  $R_i^G$ ,  $I_i^G$ , and  $u_i$  are respectively the inductance, resistance, current, and voltage of the  $i$ th DG.  $L_j^E$ ,  $R_j^E$ , and  $I_j^E$  are respectively the inductance, resistance, and current of the  $j$ th transmission line.  $C_k^N$ ,  $V_k^N$ ,  $G_k^{\text{cte}}$  and  $I_k^{\text{cte}}$  are respectively the shunt capacitance, its voltage, the constant conductance, and constant current of the  $k$ th power-consuming load. The elements  $b_{ik}^G$  and  $b_{jk}^E$  correspond to the incidence matrices, characterizing arbitrary current flows within the network.

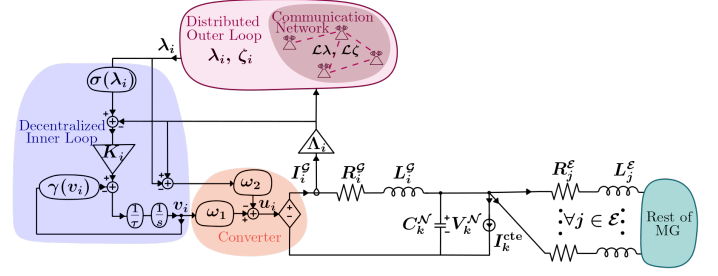


Fig. 1: Microgrid dynamics - single unit perspective.

### B. Nonlinear Nested Distributed Control Framework

Motivated by the previously proposed distributed control framework—detailed in Section II.C in [4]—this research presents a *nonlinear* control framework, imposing two nested control loops: a decentralized/primary inner loop controller that regulates current deviations with respect to a saturated set-point value, and a distributed/secondary outer loop controller that restore operating conditions. The proposed control configurations aim to ensure simultaneous achievement of the following two control objectives in steady state:

- voltage containment within pre-specified limits,
- proportional current sharing.

These control objectives are mathematically formulated as follows:

$$\begin{aligned} V_{\min} \leq V_i^G(t) \leq V_{\max}, \quad \forall t \in \mathbb{R}_{\geq 0} \\ \lim_{t \rightarrow \infty} (I_i^G/I_i^{\text{rated}} - I_l^G/I_l^{\text{rated}}) = 0, \quad \forall i, l \in \mathcal{G} \end{aligned} \quad (2)$$

where  $V_{\min}$  and  $V_{\max}$  are the minimum and maximum values of the voltage, and  $I_i^{\text{rated}}$  is the rated current of the  $i$ -th converter. In summary, the distributed controller in [4] was derived by means of the Lagrange multiplier method, where it is ensured that the system stabilizes at an equilibrium, which is the argument that minimizes a cost function. More precisely, the cost function was chosen such that current sharing is achieved in steady state when all units cooperatively decide on the optimal operating point, facilitated through communication among neighboring units. The distributed outer loop controller and the decentralized inner loop controller (local integrator for current regulation) aim to simultaneously ensure the two control objectives: voltage containment and proportional current sharing. However, the control proposal lacks stability guarantees. Thus, to facilitate obtaining a *scalable* G.E.S. certificate for the proposed DC MG in this research, we adjust the structure of the control proposal in the following ways, resulting in (3). First, we *saturate* the proportional current set-point  $\lambda$  appearing in the decentralized inner loop controller (3d) by means of a continuous strictly monotonically increasing (sigmoid) function  $\sigma(\lambda)$ , given in (3g). Second, we include the same saturation in the primal dynamics of the distributed outer loop, in (3e). Third, we update the leakage function of the regulator  $\rho(v)$  with the *smooth* and continuous nonlinear function given in (3h). Finally, to support the industrial standard (adopting proportional-integral controllers (PI)), we have included a proportional controller ( $\omega_2(\lambda_i, I_i^G)$ ) in our distributed framework, given in (3c). Note that the distributed optimizer relies on obtaining the rated current from each DG. Hence, the output of the physical network is then defined as the ratio of the DGs actual current to its rated current:  $\Lambda_i I_i^G = I_i^G / I_i^{\text{rated}}, \forall i \in \mathbb{R}^{n_i}$ . For the  $i$ th DG, the

complete control scheme is then proposed as follows:

$$u_i = V_i^{\text{set}} = \omega_1(v_i) - \omega_2(\lambda_i, I_i^G) \quad (3a)$$

$$\omega_1(v_i) = V^* + \Delta_1 \tanh(v_i / \Delta_1), \quad (3b)$$

$$\omega_2(\lambda_i, I_i^G) = \Delta_2 \tanh(k_p(\Lambda_i I_i^G - \lambda_i)), \quad (3c)$$

$$\tau_i \dot{v}_i = -\rho(v_i)v_i + k_v(\sigma(\lambda_i) - \Lambda_i I_i^G), \quad (3d)$$

$$\tau_i^p \dot{\lambda}_i = \Lambda_i I_i^G - \sigma(\lambda_i) - \sum_{j \in N_i} [a_{ij}(\zeta_i - \zeta_j) - k a_{ij}(\lambda_j - \lambda_i)], \quad (3e)$$

$$\tau_i^d \dot{\zeta}_i = \sum_{j \in N_i} a_{ij}(\lambda_i - \lambda_j), \quad (3f)$$

$$\sigma_i(\lambda_i) = \mathcal{K}_I + \Delta_I \tanh(\lambda_i / \Delta_I), \quad (3g)$$

$$\rho(v_i) = \alpha(1 + 0.5[\tanh(b(v_i - v_{\text{pos}})) - \tanh(b(v_i - v_{\text{neg}}))]). \quad (3h)$$

The distributed control framework depends on three controller states where  $\lambda_i$  and  $\zeta_i$  are the communicated states of the cyber network with respective time constants  $\tau_i^p$  and  $\tau_i^d$ , and  $v_i$  is the decentralized controller state with associated time constant  $\tau_i$ .  $u_i$  is the control actuator, constructed as a weighted sum of the two nonlinear functions  $\omega_1(v_i)$  and  $\omega_2(\lambda_i, I_i^G)$ . For voltage containment, we define:  $k_v > 0$  as the integrator gain, tuning the integration speed;  $k_p > 0$  as the proportional gain;  $V_{\max} = (1 + \mu)V_n$  and  $V_{\min} = (1 - \mu)V_n$ , for  $\mu > 0$ , as the pre-specified voltage limitations from the networks nominal voltage,  $V_n$ ;  $V^* = \frac{1}{2}(V_{\min} + V_{\max})$  as the central point within the safe voltage range;  $\Delta = \frac{1}{2}(V_{\max} - V_{\min})$  as the maximum allowed deviation from  $V^*$ ; and  $\Delta_1$  and  $\Delta_2$  are the weightings of the two functions given that  $\Delta_1 + \Delta_2 = \Delta$ .  $\tanh(\cdot)$  is a hyperbolic tangent function used to saturate the argument of  $\omega_1$  and  $\omega_2$  if they exceed the predefined limits.  $\tanh(\cdot)$  is also used in  $\rho(v_i)$  as a nonlinear leakage expression operating as an anti-wind-up function when we reach voltage saturation under the given arguments;  $v_{\text{pos}} = \Delta \tanh^{-1}[(V_{\max} - v_{\text{tol}} - V^*)/\Delta]$  and  $v_{\text{neg}} = \Delta \tanh^{-1}[(V_{\min} + v_{\text{tol}} - V^*)/\Delta]$ , where  $v_{\text{tol}}$  is the saturation tolerance,  $\alpha$  is the leakage coefficient scaling the upper bound value, and  $b$  is implemented to scale the steepness of the curve. Moreover, we use  $\tanh(\cdot)$  in  $\sigma_i(\lambda_i)$  to bound the influence of the distributed outer loop controller when entering the decentralized inner loop with  $\mathcal{K}_I = \frac{1}{2}(I_{\min}^{[\text{p.u.}]} + I_{\max}^{[\text{p.u.}]})$  and  $\Delta_I = \frac{1}{2}(I_{\max}^{[\text{p.u.}]} - I_{\min}^{[\text{p.u.}]})$ , where  $I_{\max} = (1 + \varphi)[\text{p.u.}]$  and  $I_{\min} = (1 - \varphi)[\text{p.u.}]$ , for  $\varphi \geq 0$ . Finally,  $a_{ij}$  is the *adjacency matrix* element, describing the communicating DGs where  $N_i$  is the set of the neighboring DGs in the cyber layer, and  $k$  is a positive gain.

### III. SYSTEM STEADY STATE AND STABILITY ANALYSIS

In this section, we aim to prove that the equilibrium of (4) is globally exponentially stable using singular perturbation theory and

Lyapunov theory [27]. We start by expressing the system dynamics (1)-(3) in the compact form:

$$L^G \dot{I}^G = \omega_1(v) - \omega_2(\lambda, I^G) - \beta^G V^N - R^G I^G, \quad (4a)$$

$$L^E \dot{I}^E = -\beta^E V^N - R^E I^E, \quad (4b)$$

$$C^N \dot{V}^N = \beta^{E\top} I^E + \beta^{G\top} I^G - G^{\text{cte}} V^N - I^{\text{cte}}, \quad (4c)$$

$$\tau \dot{v} = -\gamma(v) + \mathcal{K}_v(\sigma(\lambda) - \Lambda I^G), \quad (4d)$$

$$\tau_p \dot{\lambda} = \Lambda I^G - \sigma(\lambda) - \mathcal{L}\zeta - k\mathcal{L}\lambda, \quad (4e)$$

$$\tau_d \dot{\zeta} = \mathcal{L}\lambda, \quad (4f)$$

with  $L^G = \text{diag}(L_i^G) \in \mathbb{R}^{n_i \times n_i}$ ,  $I^G = \text{col}(I_i^G) \in \mathbb{R}^{n_i}$ ,  $R^G = \text{diag}(R_i^G) \in \mathbb{R}^{n_i \times n_i}$ ,  $\omega_1(v) = \text{col}(\omega_1(v_i)) \in \mathbb{R}^{n_i}$ ,  $\beta^G = [b_{ik}^G] \in \mathbb{R}^{n_i \times n_k}$ .  $L^E = \text{diag}(L_j^E) \in \mathbb{R}^{n_j \times n_j}$ ,  $I^E = \text{col}(I_j^E) \in \mathbb{R}^{n_j}$ ,  $R^E = \text{diag}(R_j^E) \in \mathbb{R}^{n_j \times n_j}$ ,  $\beta^E = [b_{jk}^E] \in \mathbb{R}^{n_j \times n_k}$ .  $C^N = \text{diag}(C_k^N) \in \mathbb{R}^{n_k \times n_k}$ ,  $V^N = \text{col}(V_k^N) \in \mathbb{R}^{n_k}$ ,  $G^{\text{cte}} = \text{diag}(G_k^{\text{cte}}) \in \mathbb{R}^{n_k \times n_k}$ ,  $I^{\text{cte}} = \text{col}(I_k^{\text{cte}}) \in \mathbb{R}^{n_k}$ ,  $v = \text{col}(v_i) \in \mathbb{R}^{n_i}$ ,  $\tau = \text{diag}(\tau_i) \in \mathbb{R}^{n_i \times n_i}$ ,  $\gamma(v) = \text{col}(\gamma_i(v_i)) \in \mathbb{R}^{n_i}$ ,  $\sigma(\lambda) = \text{col}(\sigma_i(\lambda_i)) \in \mathbb{R}^{n_i}$ ,  $\mathcal{K}_v = \text{diag}(k_v) \in \mathbb{R}^{n_i \times n_i}$ ,  $\lambda = \text{col}(\lambda_i) \in \mathbb{R}^{n_i}$ ,  $\Lambda = \text{diag}(1/I_i^{\text{rated}}) \in \mathbb{R}^{n_i \times n_i}$ ,  $\zeta = \text{col}(\zeta_i) \in \mathbb{R}^{n_i}$ ,  $\tau_p = \text{diag}(\tau_i^p) \in \mathbb{R}^{n_i \times n_i}$ ,  $\tau_d = \text{diag}(\tau_i^d) \in \mathbb{R}^{n_i \times n_i}$ . Finally,  $\mathcal{L} = [l_{ij}] \in \mathbb{R}^{n_i \times n_i}$  is the Laplacian matrix, containing the consensus properties of the communication network.

**Assumption 1.**  $\tau_p, \tau_d \gg \tau$  with  $\varepsilon = \tau$  when  $\tau$  is the slowest time constant of the fast dynamics.

Let Assumption 1 hold. Thus, we assume sufficient time-scale separation between the electrical system and the inner-loop controller (4a)-(4d), and the outer-loop controller (4e)-(4f), given below in compact form as two systems with separated timescales.

$$\dot{x} = f(x, z) \quad \text{and} \quad \varepsilon \dot{z} = g(x, z), \quad (5)$$

where  $z = \text{bcol}\{I^G, I^E, V^N, v\}$  and  $x = \text{bcol}\{\lambda, \zeta\}$ .

### A. Equilibrium Analysis

We derive the steady-state equations of (4) by expressing  $\dot{x} = 0_{n_f}$ ,  $\forall n_f \in \mathbb{R}^{(n_i+n_i)}$  and  $\dot{z} = 0_{n_g}$ ,  $\forall n_g \in \mathbb{R}^{(n_i+n_j+n_k+n_i)}$ . Hence, any steady state needs to satisfy

$$\begin{aligned} 0 &= f(\bar{v}, \bar{\lambda}, \bar{\zeta}, \bar{I}^G), \\ 0 &= g(\bar{I}^G, \bar{I}^E, \bar{V}^N, \bar{v}), \end{aligned}$$

where  $(\bar{\cdot})$  denotes the state value at its equilibrium.

**Assumption 2.** It is assumed that the communication network (represented by the Laplacian matrix  $\mathcal{L}$ ) is strongly connected and undirected.

Let Assumption 2 hold, and by leveraging the property of the Laplacian matrix where  $\mathcal{L}1_{n_i} = 0$ , the steady state operations of (4f) leads to all the DGs cooperatively agreeing upon one consensus value for the communicated state variable  $\bar{\lambda} = \lambda_s 1_{n_i}$  where  $\lambda_s$  is the singular consensus value and  $1_{n_i} = \text{col}(1) \in \mathbb{R}^{n_i}$ . When considering steady state operation of (4d) without saturated voltages-inactivated leakage function  $\rho(\bar{v}) - \Lambda \bar{I}^G$  is forced equal to  $\sigma(\bar{\lambda})$ . Subsequently, steady state operations provide consensus among the DGs in regards to the other communicated values when (4e) converge to the equilibrium and  $\bar{\zeta} = \zeta_s 1_{n_i}$ , where  $\zeta_s$  is the singular consensus value. The steady state of the electrical network (4a)-(4c) is consequently uniquely defined.

Furthermore, following the proof detailed in Section II.D in [4], our system attains optimal operations when saturation is avoided. In this

case, the controller simultaneously ensures proportional current sharing and voltage containment, provided that all neighboring DGs collaboratively determine the optimal set-point value  $\bar{\lambda}$  such that  $\Lambda \bar{I}^G = \sigma(\bar{\lambda})$  at the equilibrium, and as long as  $\rho(\bar{\lambda})$  is uniformly defined for all DGs. However, in the case of voltage saturation, the MG is steered to another optimum that fails to meet the current sharing objective at the equilibrium due to the presence of the leakage function in (4d).

### B. Singular Perturbation Theory

Following the methodology in [27], we aim to express the system dynamics in (4) as a *singular perturbation problem*, followed by Lyapunov theory, aiming to prove G.E.S. under some stability bounds. To accommodate the nested control loops, we first differentiate the dynamical system into *slow/fast* behavior/models (given in Assumption 1). Further, under a stretched time-scale ( $\mathbf{t}$ ), the singular perturbation problem is partitioned into the *reduced-* and *boundary layer* systems. By proposing two separate Lyapunov candidates for the two time-scaled systems, we aim to prove G.E.S. of the individual systems. This facilitates finding a composite Lyapunov function for the singularly perturbed system as a weighted sum of the two Lyapunov candidates, used to conclude on G.E.S. of the *full* system.

**Theorem 1. (Singular Perturbed Problem)** Consider the closed loop dynamics in (4), and let

$$\begin{aligned} \Omega_1(\tilde{x}, \tilde{y}^4 + H^4(\tilde{x})) &\triangleq \omega_1(\tilde{y}^4 + \hat{H}^4(\tilde{x})) - \omega_1(h^4(\tilde{x})), \\ \Omega_2(\tilde{x}, \tilde{y}^1 + H^1(\tilde{x})) &\triangleq \omega_2(\tilde{x}, \tilde{y}^1 + \hat{H}^1(\tilde{x})) - \omega_2(\tilde{x}, h^1(\tilde{x})), \\ \Gamma(\tilde{x}, \tilde{y}^4 + H^4(\tilde{x})) &\triangleq \gamma(\tilde{y}^4 + \hat{H}^4(\tilde{x})) - \gamma(h^4(\tilde{x})), \\ \Sigma(\tilde{\lambda}) &\triangleq \sigma(\tilde{\lambda}) - \sigma(\bar{\lambda}), \\ \mathcal{Q}_s &\triangleq \text{bdiag}\{\tau_p, \tau_d\} > 0, \quad \mathcal{P}_s \triangleq \text{bdiag}\{k\mathcal{L}, \mathcal{B}_\zeta\} > 0, \\ \mathcal{J}_s &\triangleq \begin{bmatrix} \mathbf{0}_{n_i \times n_i} & -\mathcal{L} \\ \mathcal{L} & \mathbf{0}_{n_i \times n_i} \end{bmatrix}, \quad \kappa_1 \triangleq \begin{bmatrix} \mathbf{1}_{n_i \times n_i} & \mathbf{0}_{n_i \times n_i} \\ \mathbf{0}_{n_i \times n_i} & \mathbf{0}_{n_i \times n_i} \end{bmatrix}, \\ \mathcal{Q}_f &\triangleq \text{bdiag}\{L^G, L^E, C^N\} > 0, \quad \mathcal{P}_f \triangleq \text{bdiag}\{R^G, R^E, G^{\text{cte}}\} > 0, \\ \mathcal{J}_f &\triangleq \begin{bmatrix} \mathbf{0}_{n_i \times n_i} & \mathbf{0}_{n_i \times n_j} & -\beta^G \\ \mathbf{0}_{n_j \times n_i} & \mathbf{0}_{n_j \times n_j} & -\beta^E \\ \beta^{G\top} & \beta^{E\top} & \mathbf{0}_{n_k \times n_k} \end{bmatrix}, \\ \kappa_2 &\triangleq \begin{bmatrix} \mathbf{1}_{n_i \times n_i} & \mathbf{0}_{n_i \times n_j} & \mathbf{0}_{n_i \times n_k} \\ \mathbf{0}_{n_j \times n_i} & \mathbf{0}_{n_j \times n_j} & \mathbf{0}_{n_j \times n_k} \\ \mathbf{0}_{n_k \times n_i} & \mathbf{0}_{n_k \times n_j} & \mathbf{0}_{n_k \times n_k} \end{bmatrix}, \end{aligned}$$

where  $h(x) = \text{bcol}\{h_i^1(x), h_j^2(x), h_k^3(x), h_i^4(x)\}$ ,  $\forall i \in \mathcal{G}, \forall j \in \mathcal{E}, \forall k \in \mathcal{N}$ , is the unique solution of  $0 = g(x, h(x))$ ;  $\tilde{y} \triangleq \text{bcol}\{\tilde{z} - H(\tilde{x})\}$ ;  $H(\tilde{x}) \triangleq \text{bcol}\{\hat{H}(\tilde{x}) - h(\tilde{x})\}$ ;  $\hat{H}(\tilde{x}) \triangleq \text{bcol}\{h(\tilde{x} + \bar{x})\}$ . Suppose that  $\Omega_1(\tilde{x}, \tilde{y}^4 + H^4(\tilde{x}))$ ,  $\Omega_2(\tilde{x}, \tilde{y}^1 + H^1(\tilde{x}))$ , and  $\Gamma(\tilde{x}, \tilde{y}^4 + H^4(\tilde{x}))$  are Lipschitz and element-wise strictly monotonically increasing sigmoid functions in  $\tilde{y}^4$  and  $\tilde{y}^1$  respectively. The two separated systems in (5) can then be expressed as the singular perturbed problem under the stretched timescale  $\mathbf{t} = (t/\varepsilon)$ , where  $f(\tilde{x}, H(\tilde{x}))$  and  $\hat{g}(\tilde{x}, \tilde{y} + H(\tilde{x}))$

represent the reduced and boundary layer systems, respectively.

$$\hat{f}(\tilde{x}, H(\tilde{x})) : \begin{cases} \mathcal{Q}_s \dot{\tilde{x}} = [\mathcal{J}_s - \mathcal{P}_s] \tilde{x} + \kappa_1 [\Lambda H_1(\tilde{x}) - \Sigma(\tilde{\lambda})] \end{cases} \quad (7a)$$

$$\hat{g}(\tilde{x}, \tilde{y} + H(\tilde{x})) : \quad (7b)$$

$$\begin{cases} \mathcal{Q}_f \partial \tilde{y}_f / \partial \mathbf{t} = [\mathcal{J}_f - \mathcal{P}_f] (\tilde{y}_f + H_f(\tilde{x})) \\ \quad + \kappa_2 [\Omega_1(\tilde{x}, \tilde{y}_4 + H_4(\tilde{x})) - \Omega_2(\tilde{x}, \tilde{y}_1 + H_1(\tilde{x}))] \\ \tau \partial \tilde{y}_4 / \partial \mathbf{t} = -\Gamma(\tilde{x}, \tilde{y}_4 + H_4(\tilde{x})) + \mathcal{K}_v [\Sigma(\tilde{\lambda}) - \Lambda(\tilde{y}_1 + H_1(\tilde{x}))] \\ \quad - \mathcal{B}_v (\tilde{y}_4 + H_4(\tilde{x})) \end{cases}$$

where  $\tilde{y}_f \triangleq \text{bcol}\{\tilde{y}^1, \tilde{y}^2, \tilde{y}^3\}$ ;  $H_f(\tilde{x}) \triangleq \text{bcol}\{H^1(\tilde{x}), H^2(\tilde{x}), H^3(\tilde{x})\}$ .

*Proof.* First, we consider  $\varepsilon = \tau$  to be very small such that the velocity of  $\dot{z} \propto (1/\varepsilon)$  behaves instantaneously fast where  $z$  rapidly converges to the root of  $0 = g(x, z)$ . Hence, the fast system in (4a)-(4d) quickly reaches a *quasi-steady state* given the instantaneous fast dynamics,  $h(x)$ , which are obtained by solving  $0 = g(x, h(x))$  for  $h(x)$  as a function of  $x$ ; as indicated in (8).<sup>1</sup>

$$0 = \begin{bmatrix} \omega_1(h^4(x)) - \omega_2(\lambda, h^1(x)) - \beta^g h^3(x) - R^g h^1(x) \\ -\beta^e h^3(x) - R^e h^2(x) \\ \beta^g h^1(x) + \beta^e h^2(x) - G^{\text{cte}} h^3(x) - I^{\text{cte}} \\ -\rho(h^4(x)) + K_v(\sigma(\lambda) - \Lambda h^1(x)) \end{bmatrix}, \quad (8)$$

such that  $h(x) = \begin{bmatrix} h_i^1(x) \\ h_i^2(x) \\ h_i^3(x) \\ h_i^4(x) \end{bmatrix}, \quad \forall i \in \mathcal{G}, \forall j \in \mathcal{E}, \forall k \in \mathcal{N}.$

We further define  $y = \text{bcol}\{y_i^1, y_j^2, y_k^3, y_i^4\}$  as the error between the actual fast dynamics and the quasi-steady state:  $y^b \triangleq \text{bcol}\{z^b - h^b(x)\}, \forall b \in [1, 2, 3, 4]$ . Moreover, to facilitate applying the Lyapunov theory on the two time-separated systems, we express the system states using their incremental variables  $\tilde{z} = z - \bar{z}$ ,  $\tilde{y} = y - \bar{y}$  and  $\tilde{x} = x - \bar{x}$ . Thus, we express the incremental *real* fast dynamics as  $\tilde{z} \triangleq \tilde{y} + h(\tilde{x} + \bar{x}) - h(\bar{x}) = \tilde{y} + H(\tilde{x})$  when noticing that  $\bar{z} = h(\bar{x})$ , such that  $\bar{y} = 0$ . Following *Assumption 1*, we express the fast and slow dynamical models as

$$f(\tilde{x}, \tilde{z}) : \begin{cases} \mathcal{Q}_s \dot{\tilde{x}} = [\mathcal{J}_s - \mathcal{P}_s] \tilde{x} + \kappa_1 [\Lambda \tilde{z}^1 - \Sigma(\tilde{\lambda})], \end{cases} \quad (9a)$$

$$g(\tilde{x}, \tilde{z}) : \begin{cases} \mathcal{Q}_f \dot{\tilde{z}}_f = [\mathcal{J}_f - \mathcal{P}_f] \tilde{z}_f + \kappa_2 [\Omega_1(\tilde{x}, \tilde{z}^4) - \Omega_2(\tilde{x}, \tilde{z}^1)] \\ \tau \dot{\tilde{z}}^4 = -\Gamma(\tilde{x}, \tilde{z}^4) + \mathcal{K}_v [\Sigma(\tilde{\lambda}) - \Lambda \tilde{z}^1] - \mathcal{B}_v \tilde{z}^4. \end{cases} \quad (9b)$$

For compactness, we have defined the following for the slow model; the cyber inertia matrix  $\mathcal{Q}_s$ ; the symmetrical cyber resistance matrix  $\mathcal{P}_s$ ; and the interconnection matrix  $\mathcal{J}_s$  and allocation matrix  $\kappa_1$ —with its dynamics previously defined in *Theorem 1*. Moreover, for the fast model, we have defined the following; the reduced fast state vector  $\tilde{z}_f \triangleq \text{bcol}\{\tilde{z}^1, \tilde{z}^2, \tilde{z}^3\}$ , the physical inertia matrix  $\mathcal{Q}_f$ ; the physical resistance matrix  $\mathcal{P}_f$ ; and the interconnection matrix  $\mathcal{J}_f$  and allocation matrix  $\kappa_2$ —dynamics defined in *Theorem 1*.

For mathematical purposes, we have introduced an additional leakage constant  $\mathcal{B}_\zeta$ , ensuring  $\mathcal{P}_s$  to be a fully diagonal matrix. Note that  $\mathcal{B}_\zeta$  does not need to compensate for any off-diagonal elements in the cyber resistance matrix. Hence, we choose the value to be arbitrarily small not to hinder the capability of achieving consensus for an optimal value of  $\lambda$ . Moreover, we have implemented an

additional constant leakage  $\mathcal{B}_v$  subtracted in the slow model to bring dissipation and improve the stability margins. These adjustments are further discussed in the following case studies in Section IV.

The time-separated systems in (9) are then expressed as the *singular perturbation problem* in (7), partitioned into the reduced system (7a) and the boundary layer system (7b) divided under the stretched timescale  $\mathbf{t} = (t/\varepsilon)$  where  $t$  is the time when  $\varepsilon \approx 0$ . Thus, the slow model (9a) will instantaneously achieve a quasi-steady state as the fast dynamics are considered instantaneously fast, such that  $y \approx 0$  in the reduced system (7a).  $\square$

### C. Lyapunov Stability Analysis

**Theorem 2.** (*Global Exponential Stability*) *The singular perturbed problem in (7) is guaranteed G.E.S. under the following bounds.*

$$\begin{aligned} -[\tilde{y}^1 + H^1(\tilde{x})]^\top \Omega_2(\tilde{x}, \tilde{y}^1 + H^1(\tilde{x})) &\leq -\nu \|\tilde{y}^1\|^2, \\ -\Omega_1(\tilde{x}, \tilde{y}^4 + H^4(\tilde{x}))^\top [\mathcal{K}_v \Lambda]^{-1} \mathcal{K}_v \Sigma(\tilde{\lambda}) &\leq -\chi \|\tilde{y}^4\|^2, \\ -\Omega_1(\tilde{x}, \tilde{y}^4 + H^4(\tilde{x}))^\top [\mathcal{K}_v \Lambda]^{-1} \\ &\quad \times [\Gamma(\tilde{x}, \tilde{y}^4 + H^4(\tilde{x})) - \mathcal{B}_v (\tilde{y}^4 + H^4(\tilde{x}))] \leq -\phi \|\tilde{y}^4\|^2, \end{aligned}$$

for some  $(\nu, \chi, \phi) \in \mathbb{R} > 0$ . Moreover, let  $\mathcal{M}(\lambda) \triangleq [\sigma(\lambda) - \Lambda h^1(\lambda)]$ . Thus, if  $\mathcal{M}(\lambda)$  is strictly monotonically increasing; that is,

$$\frac{1}{2} [\nabla^\top \mathcal{M}(\lambda) + \nabla \mathcal{M}(\lambda)] > 0, \quad (10)$$

then, there exists  $\varepsilon^* > 0$  such that for all  $\tau_p, \tau_d \gg \varepsilon^*$  the system in (4) is globally exponentially stable.

*Proof.* Considering the singularly perturbed system in (7), we define the subsequent Lyapunov candidates for the boundary layer system and the reduced system, to ensure global exponential stability of the two time-separated systems. First, we express the Lyapunov candidate for the boundary layer system as

$$\begin{aligned} V_f(\tilde{x}, \tilde{y}) &= \frac{1}{2} [\tilde{y}_f + H_f(\tilde{x})]^\top \mathcal{Q}_f [\tilde{y}_f + H_f(\tilde{x})] \\ &\quad + \int_0^{\tilde{y}^4} [\omega_1(\eta + \hat{H}^4(\tilde{x})) - \omega_1(h^4(\tilde{x}))]^\top \tau [\mathcal{K}_v \Lambda]^{-1} \partial \eta > 0. \end{aligned} \quad (11)$$

Per *Theorem 1*,  $\mathcal{Q}_f > 0$ , thus ensuring the first term to be positive. By definition,  $\mathcal{K}_v$  and  $\Lambda$  are positive definite, and  $\omega_1(\cdot)$  is a strictly monotonically increasing function in  $\tilde{y}^4$ , such that the integral is guaranteed to be positive. Taking the time derivative of the Lyapunov function then gives

$$\begin{aligned} \dot{V}_f(\tilde{x}, \tilde{y}) &= \nabla^\top V_f(\tilde{x}, \tilde{y}) \dot{\tilde{y}} \\ &= -[\tilde{y}_f + H_f(\tilde{x})]^\top \mathcal{P}_f [\tilde{y}_f + H_f(\tilde{x})] \\ &\quad + [\tilde{y}^1 + H^1(\tilde{x})]^\top (\Omega_1(\tilde{x}, \tilde{y}^4 + H^4(\tilde{x})) - \Omega_2(\tilde{x}, \tilde{y}^1 + H^1(\tilde{x}))) \\ &\quad + \Omega_1(\tilde{x}, \tilde{y}^4 + H^4(\tilde{x}))^\top \tau [\mathcal{K}_v \Lambda]^{-1} \dot{\tilde{y}}^4 \\ &= -[\tilde{y}_f + H_f(\tilde{x})]^\top \mathcal{P}_f [\tilde{y}_f + H_f(\tilde{x})] \\ &\quad - [\tilde{y}^1 + H^1(\tilde{x})]^\top \Omega_2(\tilde{x}, \tilde{y}^1 + H^1(\tilde{x})) \\ &\quad - \Omega_1(\tilde{x}, \tilde{y}^4 + H^4(\tilde{x}))^\top [\mathcal{K}_v \Lambda]^{-1} \mathcal{K}_v \Sigma(\tilde{\lambda}) \\ &\quad - \Omega_1(\tilde{x}, \tilde{y}^4 + H^4(\tilde{x}))^\top [\mathcal{K}_v \Lambda]^{-1} \\ &\quad \times [\Gamma(\tilde{x}, \tilde{y}^4 + H^4(\tilde{x})) - \mathcal{B}_v (\tilde{y}^4 + H^4(\tilde{x}))] \leq 0, \end{aligned} \quad (12)$$

where we have used the skew-symmetry of the interconnection matrix  $\mathcal{J}_f$  in the first equality. The last inequality of (12) is obtained by noticing; the first term is negative definite as  $\mathcal{P}_f > 0$ ;

<sup>1</sup>In this system, the fast dynamics exclusively depend on the slow state  $\lambda$ . However, for the generality of this proof, we keep  $h(x)$  formulated as a function of all potential slow states.

$[\tilde{y}^1 + H^1(\tilde{x})]^\top \Omega_2(\tilde{x}, \tilde{y}^1 + H^1(\tilde{x}))$  is strictly monotonically increasing in  $\tilde{y}^1$  by construction when  $\mathcal{K}_p > 0$ ; both  $\Omega_1(\tilde{x}, \tilde{y}^4 + H^4(\tilde{x}))$  and  $\Gamma(\tilde{x}, \tilde{y}^4 + H^4(\tilde{x}))$  are strictly monotonically increasing in  $\tilde{y}^4$ . Hence, we bound the last terms in (12) as follows

$$-[\tilde{y}^1 + H^1(\tilde{x})]^\top \Omega_2(\tilde{x}, \tilde{y}^1 + H^1(\tilde{x})) \leq -\nu \|\tilde{y}^1\|^2, \quad (13a)$$

$$-\Omega_1(\tilde{x}, \tilde{y}^4 + H^4(\tilde{x}))^\top [\mathcal{K}_v \Lambda]^{-1} \mathcal{K}_v \Sigma(\tilde{\lambda}) \leq -\chi \|\tilde{y}^4\|^2, \quad (13b)$$

$$-\Omega_1(\tilde{x}, \tilde{y}^4 + H^4(\tilde{x}))^\top [\mathcal{K}_v \Lambda]^{-1} \times [\Gamma(\tilde{x}, \tilde{y}^4 + H^4(\tilde{x})) - \mathcal{B}_v(\tilde{y}^4 + H^4(\tilde{x}))] \leq -\phi \|\tilde{y}^4\|^2. \quad (13c)$$

for some scalars  $(\nu, \chi, \phi) > 0$ . Note that even though the boundary layer system depends on both slow and fast dynamics ( $V_f(\tilde{x}, \tilde{y})$ ), the slow states entering the boundary layer system are considered frozen variables due to sufficient time-scale separation. Thus, the time derivative of the Lyapunov function along the trajectories of the boundary layer system only concerns the change in the error between the real fast dynamics and the instantaneous fast dynamics ( $\tilde{y}$ ) with respect to time. Hence, we allow the Lyapunov function to depend on the slow variables  $\tilde{x}$ , and conclude on global asymptotic stability (G.A.S.) for the boundary layer system. Furthermore, to conclude G.E.S. we first want to upper bound the Lyapunov function by  $V_f(\tilde{x}, \tilde{y}) \leq c \|\tilde{y}\|^2$ . Then, we use the fact that  $\Omega_1(\tilde{x}, \tilde{y}^4 + H^4(\tilde{x}))$  adheres to the Lipschitz condition, thus allowing us to contain the value as follows

$$\int_0^{\tilde{y}^4} [\omega_1(\eta + \hat{H}^4(\tilde{x})) - \omega_1(h^4(\tilde{x}))]^\top \partial \eta \leq L \int_0^{\tilde{y}^4} \eta \partial \eta,$$

for some scalar  $\eta > 0$  and  $L > 0$  is the Lipschitz constant. Therefore,  $V_f(\tilde{x}, \tilde{y}) \leq V_1(\tilde{y})$  with  $V_1(\tilde{y}) \triangleq \frac{1}{2} \tilde{y}_f^\top \mathcal{Q}_f \tilde{y}_f + \frac{1}{2} L \tilde{y}^4{}^2 = \frac{1}{2} \tilde{y}^\top \mathcal{Q}_f^* \tilde{y} \leq \Upsilon_{\max}(\mathcal{Q}_f^*) \|\tilde{y}\|^2$  and  $\mathcal{Q}_f^* \triangleq \text{bdiag}\{\mathcal{Q}_f, L\} > 0$  with  $\Upsilon_{\max}$  being the maximum eigenvalue of  $\mathcal{Q}_f^*$ . Hence, we have

$$V_f(\tilde{x}, \tilde{y}) \leq \Upsilon_{\max}(\mathcal{Q}_f^*) \|\tilde{y}\|^2. \quad (14)$$

Furthermore, the time derivative of the Lyapunov function along the trajectories of the fast system is bounded by

$$\dot{V}_f(\tilde{x}, \tilde{y}) \leq -\Upsilon_{\min}(\mathcal{P}_f^*) \|\tilde{y}\|^2, \quad (15)$$

for  $\Upsilon_{\min}$  being the minimum eigenvalue of  $\mathcal{P}_f^* = \text{bdiag}\{\mathcal{P}_f, \Phi\}$  where we have incorporated (13) in (12) to define  $\mathcal{P}_f^*$ .

$$\mathcal{P}_f^* \triangleq \text{bdiag}\{(R^G + \nu), R^E, G^{\text{cte}}, (\chi + \Phi)\}$$

Finally, using (14) and (15), we conclude G.E.S. with the convergence rate

$$\epsilon = 2 \frac{\Upsilon_{\min}(\mathcal{P}_f^*)}{\Upsilon_{\max}(\mathcal{Q}_f^*)}.$$

Considering the reduced system (7a), the Lyapunov candidate and its derivative along the trajectories of the slow system are proposed as

$$W_s(\tilde{x}) = \frac{1}{2} \tilde{x}^\top \mathcal{Q}_s \tilde{x} > 0, \quad (16a)$$

$$\begin{aligned} \dot{W}_s(\tilde{x}) &= \nabla^\top W_s(\tilde{x}) \dot{\tilde{x}} \\ &= -\tilde{x}^\top \mathcal{P}_s \tilde{x} - (\lambda - \bar{\lambda})^\top [\mathcal{M}(\lambda) - \mathcal{M}(\bar{\lambda})] \leq 0. \end{aligned} \quad (16b)$$

Per *Theorem 1*  $\mathcal{Q}_s$  is a positive definite matrix, thus guaranteeing  $W_s > 0$ . Furthermore, when assessing its time derivative, the last inequality in (16b) is satisfied as  $\mathcal{P}_s > 0$ , while assuming  $\mathcal{M}(\lambda) = [\sigma(\lambda) - \Lambda h^1(\lambda)]$  to be strictly monotonically increasing.

Hence, we conclude G.E.S. for the reduced system when  $\mathcal{M}(\lambda)$  is bounded by the following constraint

$$-(\lambda - \bar{\lambda})^\top [\mathcal{M}(\lambda) - \mathcal{M}(\bar{\lambda})] < -\gamma \|\bar{\lambda}\|^2, \quad (17)$$

for some scalar  $\gamma > 0$ .

Since both  $V_f(\tilde{x}, \tilde{y})$  and  $W_s(\tilde{x})$  are positive definite and radially unbounded, we conclude G.E.S. of the reduced and the boundary layer system. Thus, the singularly perturbed system in (7), satisfies all conditions given in *Theorem 11.4* in [27] and *Theorem 2* and the system in (4) is globally exponentially stable as there exists  $\epsilon^* > 0$  for all  $\tau_p, \tau_d \gg \epsilon^*$ .  $\square$

In the general case, the condition in (10) might be a bit complicated to verify as  $\mathcal{M}(\lambda)$  is dense. When considering a fully interconnected system operating under saturated voltages, the activated leakage function introduces interdependencies among neighboring DGs and loads. By considering  $0 = g(I^G, I^E, V^N, v)$  we obtain following expression for  $v$

$$v = \omega_1^{-1} [(\beta^G \theta \beta^{G^\top} + \mathcal{R}^G) I^G + \beta^G \theta I^{\text{cte}} + \omega_2(\lambda, I^G)], \quad (18)$$

with  $\theta = [\beta^{E^\top} \mathcal{R}^{E-1} \beta^E + G^{\text{cte}}]^{-1}$ .

This emphasizes that  $\rho(v)$  depends on both incidence matrices  $\beta^G$  and  $\beta^E$  and the value of  $\rho(v_i)$  additionally depends on the cross-coupled current values  $(I_i^G, \dots, I_n^G)$ . In fact,  $\beta^{E^\top} \mathcal{R}^{E-1} \beta^E$  is indeed the *non-diagonal*  $Y_{\text{bus}}$  of the electrical network, emphasizing the dependence on neighboring currents. Hence, when the leakage function is activated, each of the local instantaneous fast dynamics (with respect to the instantaneous currents; i.e.,  $h^1(\lambda)$ ) is a function of its neighboring  $\lambda$ -values; that is,

$$\Lambda h_i^1(\lambda_1, \dots, \lambda_n) \quad \forall i \in \mathbb{R}^{n_i}.$$

In (19) we compute the symmetrical part of  $\frac{\partial \mathcal{M}(\lambda)}{\partial \lambda}$ , revealing the inter-dependencies in the off-diagonal elements.

$$\left. \frac{\partial \mathcal{M}(\lambda)}{\partial \lambda} \right|_{\text{sym}} = \begin{bmatrix} \frac{\partial(\sigma(\lambda) - \Lambda h_1^1(\lambda))}{\partial \lambda_1} & \dots & \frac{-\partial \Lambda h_1^1(\lambda)}{\partial \lambda_{n_1}} \\ \vdots & \ddots & \vdots \\ \frac{-\partial \Lambda h_{n_i}^1(\lambda)}{\partial \lambda_1} & \dots & \frac{\partial(\sigma(\lambda) - \Lambda h_{n_i}^1(\lambda))}{\partial \lambda_{n_i}} \end{bmatrix} \quad (19)$$

Therefore, ensuring the stability condition in (10) would indeed be significantly simplified if that matrix is dominated by its diagonal elements. With this in mind, we introduce the following *Corollary* to simplify the application of our stability result.

**Corollary 1.** *Tuning the leakage coefficient,  $\alpha$ , to a sufficiently small value minimizes the inter-dependencies of  $h^1(\lambda)$  such that  $\left. \frac{\partial \mathcal{M}}{\partial \lambda} \right|_{\text{sym}}$  approximately becomes a (positive) diagonal matrix. Moreover, adjusting some electrical specifications (more precisely, the rated currents or load conductance) ensures positive diagonal dominance. Thus, ensuring  $\mathcal{M}(\lambda)$  to be strictly monotonically increasing.*

*Proof.* Positive definiteness of  $\left. \frac{\partial \mathcal{M}(\lambda)}{\partial \lambda} \right|_{\text{sym}}$  is guaranteed when the matrix-diagonal is dominant and each diagonal element is positive definite. In (3d), the leakage function is introduced to ensure the feasibility of the equilibrium under saturated conditions. Due to the time-scale separation at the border between the nested loops, both separated systems maintain a convenient mathematical structure, and the introduced leakage coefficient  $\alpha$  in (3h) can be fine-tuned without impacting the stability conditions. Consequently, we guarantee



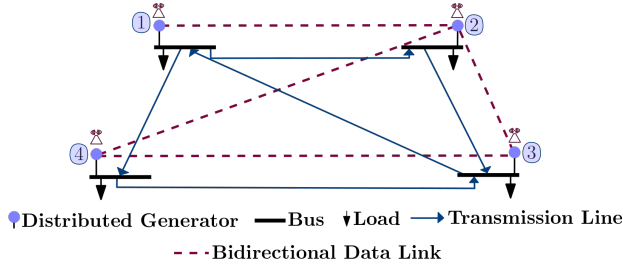


Fig. 2: Case Specific Microgrid

TABLE I: Parameter values for case-specific MG

Generator specifications; $i \in \mathcal{G}$				
$I_i^{\text{rated}}$ [A]	12	4	8	8
$R_i^{\mathcal{G}}$ [p.u.], $L_i^{\mathcal{G}}$ [p.u.]	0.5	0.4	0.55	0.6
Load specifications; $k \in \mathcal{N}$				
$C_k^{\mathcal{N}}$ [F]	$22 \times 10^{-3}$			
$1/G_k^{\mathcal{N}}$ [ $\Omega$ ]	40	30	30	30
$I_k^{\text{cte}}$ [A]	1	1.2	0.8	1
Transmission lines specifications; $j \in \mathcal{E}$				
$R_j^{\mathcal{E}}$ [p.u.], $L_j^{\mathcal{E}}$ [p.u.]	1	2	2	1

diagonal dominance and positive definiteness of (19) by tuning  $\alpha$  to a sufficiently small value such that  $\frac{\partial \mathcal{M}(\lambda)}{\partial \lambda}|_{\text{sym}}$  is solely determined by its diagonal elements.

By construction,  $\sigma(\lambda)$  is strictly monotonically increasing in  $v$ , and the solution of (8) for  $h^1(\lambda)$  gives a monotonically increasing function for some sufficiently small  $\alpha$ . However the subtraction  $\frac{\partial \sigma(\lambda) - \partial \Lambda h^1(\lambda)}{\partial \lambda}$  is not guaranteed to be monotonically increasing. Hence, for a sufficient scale of the system, the condition  $\frac{\partial \sigma(\lambda)}{\partial \lambda} > \frac{\partial \Lambda h^1(\lambda)}{\partial \lambda}$  is guaranteed for sufficiently higher-rated currents (i.e., for a sufficiently small  $\Lambda$ ). Thus, the diagonal elements of  $\frac{\partial \mathcal{M}}{\partial \lambda}|_{\text{sym}}$  are positive definite, such that *Corollary 1* and the stability condition in (17) are satisfied, and we conclude upon G.E.S. for the reduced system.  $\square$

#### IV. CASE STUDIES

The control framework in (3) is tested by means of time-domain simulations in MATLAB/Simulink on a 48-volt DC network admitting the dynamics in (1). The DC microgrid is powered by 4 DGs, interconnected electrically and through communication links according to the interconnection patterns depicted in Fig.2. The specifications of the generators, loads, and transmission lines are given in Table I, where all resistance ( $R$ ) and inductance ( $L$ ) values are specified in per unit (p.u) on a  $(0.15\Omega, 300\mu H)$  base. The control parameters;  $\tau = 1s$  and  $\tau_p, \tau_d = 10s$ , are selected to satisfy *Assumption 1* with  $k = 10$  and  $b = 5$ . The subsequent case studies discuss acceptable tuning values of  $\alpha, \mathcal{K}_v$ . The maximum allowed voltage deviation from the nominal voltage,  $V_n = 48V$ , is 5%;  $V_{\max} = 1.05[p.u]$ . Moreover, for voltage containment, we apply  $\Delta_1 = \Delta$  and  $\Delta_2 = 0$ , i.e., we simulate the system solely with the integral controller and further discuss the system response with the PI in Section IV-D.

*Corollary 1* highlights that achieving global exponential stability guarantees for large-signal disturbances is highly dependent on reducing the inter-dependencies in the electrical system such that  $\mathcal{M}(\lambda)$  is strictly monotonically increasing. Accordingly, through the subsequent case studies, we aim to find adequate tuning of our controller – tested for various electrical system parameters – to guarantee G.E.S. following the stability conditions in *Theorem 2*

while striving to satisfy optimal steady-state operation of the DC microgrid, where both voltage containment and proportional current sharing are maintained, as established in Section III-A.

##### A. Case Study: Verification of Corollary 1 and Assumption 2

We conduct an initial case study to tune the controller, ensuring compliance with *Corollary 1* for G.E.S. under large-signal disturbances. The *Corollary* requires reducing the electrical inter-dependencies,  $\frac{\partial h_i^1(\lambda_j)}{\partial \lambda_j}$ , such that  $\frac{\partial \mathcal{M}(\lambda)}{\partial \lambda}$  is positive definite, dominated by its positive diagonal elements; i.e.,  $\frac{\partial \sigma(\lambda)}{\partial \lambda} > \frac{\partial \Lambda h^1(\lambda)}{\partial \lambda}$ . Fig. 3 plots these functions for varying  $\alpha$  (tuning the leakage function  $\rho(v)$ ) and electrical parameter settings. Per (18), increasing  $G^{\text{cte}}$  reduces  $\theta$ , thereby minimizing the inter-dependencies, while *Corollary 1* notes that higher rated currents enhances diagonal dominance of  $\frac{\partial \mathcal{M}(\lambda)}{\partial \lambda}$ . Thus, the G.E.S. certificate requires careful control tuning and is sensitive to the electric system parameters.

Fig. 3(a) shows that for  $\alpha = V_{\max}$ , G.E.S. is not guaranteed, as  $\frac{\partial \sigma(\lambda) - \partial \Lambda h^1(\lambda)}{\partial \lambda}$  is not continuously positive definite due to the active leakage function. In contrast, Fig. 3(b) indicates positive definiteness, but increasing  $I^{\text{rated}}$  strengthens both diagonal and off-diagonal elements, making it unclear if the diagonal sufficiently dominates to ensure G.E.S. Fig. 3(c) resolves this by imposing a sufficiently small  $\rho(v)$  and a set of specific system parameters, achieving negligible inter-dependencies and a strictly positive definite diagonal – ensuring consistently compliance with *Corollary 1*.

##### B. Case Study: Control Performance under Stability Constraints

This case study evaluates the performance and effectiveness of the proposed control framework in (4) when applied to the case-specific DC microgrid. The following simulations are included to evaluate the controller ability to ensure voltage containment and proportional current sharing across various operating conditions, including both small- and large-signal disturbances. The distributed controller activates at  $t = 5s$ . Load changes are imposed as follows: at  $t = 50s$  the constant current at Load 1 increases by 25%; at  $t = 75s$  the constant conductance at Load 3 increases by 15%; and at  $t = 100s$  the constant current at Load 1 decreases by 15%. To test the scalability, DG1 is disconnected at  $t = 200s$  and reconnected at  $t = 300s$ , and Load 4 is disconnected during  $t \in [370, 410]$ . The simulations first depict the impact of varying  $\alpha$  ( $\rho(v)$ ) and  $\mathcal{K}_v$  on the convergence rate, as shown in Fig. 4. Secondly, the system performance is evaluated in 5, assessing the controller ability to ensure convergence to *almost* optimal steady state operations. For the subsequent case studies (Section IV-B, IV-C, and IV-D), the system parameters are updated per *Corollary 1* (tuning obtained in Section IV-A), setting  $I^{\text{rated}} = 1.5 \times I^{\text{rated}*}$  and  $G^{\text{cte}} = 5 \times G^{\text{cte}*}$ , where  $(\cdot)^*$  represents the values in Table I. Moreover, we set  $\mathcal{B}_\zeta = 1e^{-3}$  and  $\mathcal{B}_v = 1e^{-5}$  to improve the stability margins for smaller time-scale separations, further discussed in Section IV-C. According to Section III-A, the system converges to optimal equilibrium when the decentralized controller states ( $v$ -values) stay within saturation limits ( $\pm 3$ ), avoiding voltage saturation and activation of the leakage function, thus ensuring consensus and optimal *optimal* current sharing. However, the simulations indicate that  $\alpha$  and  $\mathcal{K}_v$  significantly affect  $v$ -values and convergence rates. In Fig. 4, the first two rows show that higher  $\mathcal{K}_v$  values drive the system away from the optimal equilibrium by pushing

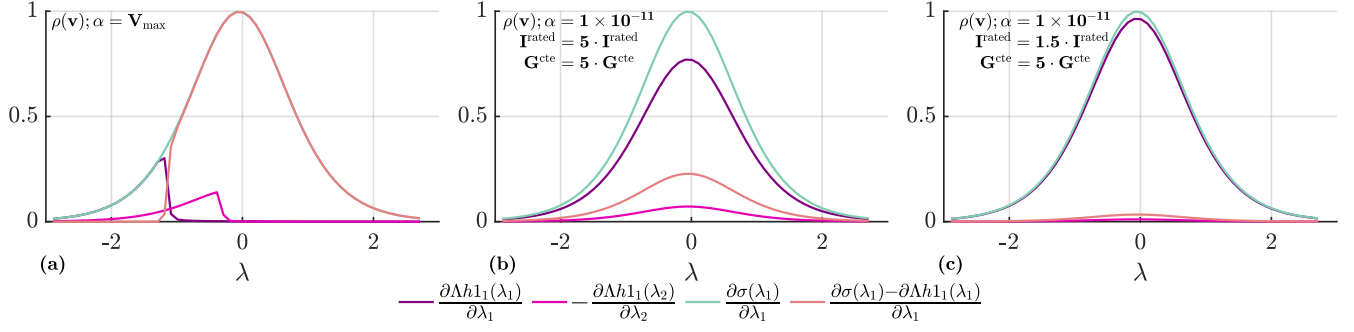


Fig. 3: Hyperbolic tangent functions under consideration

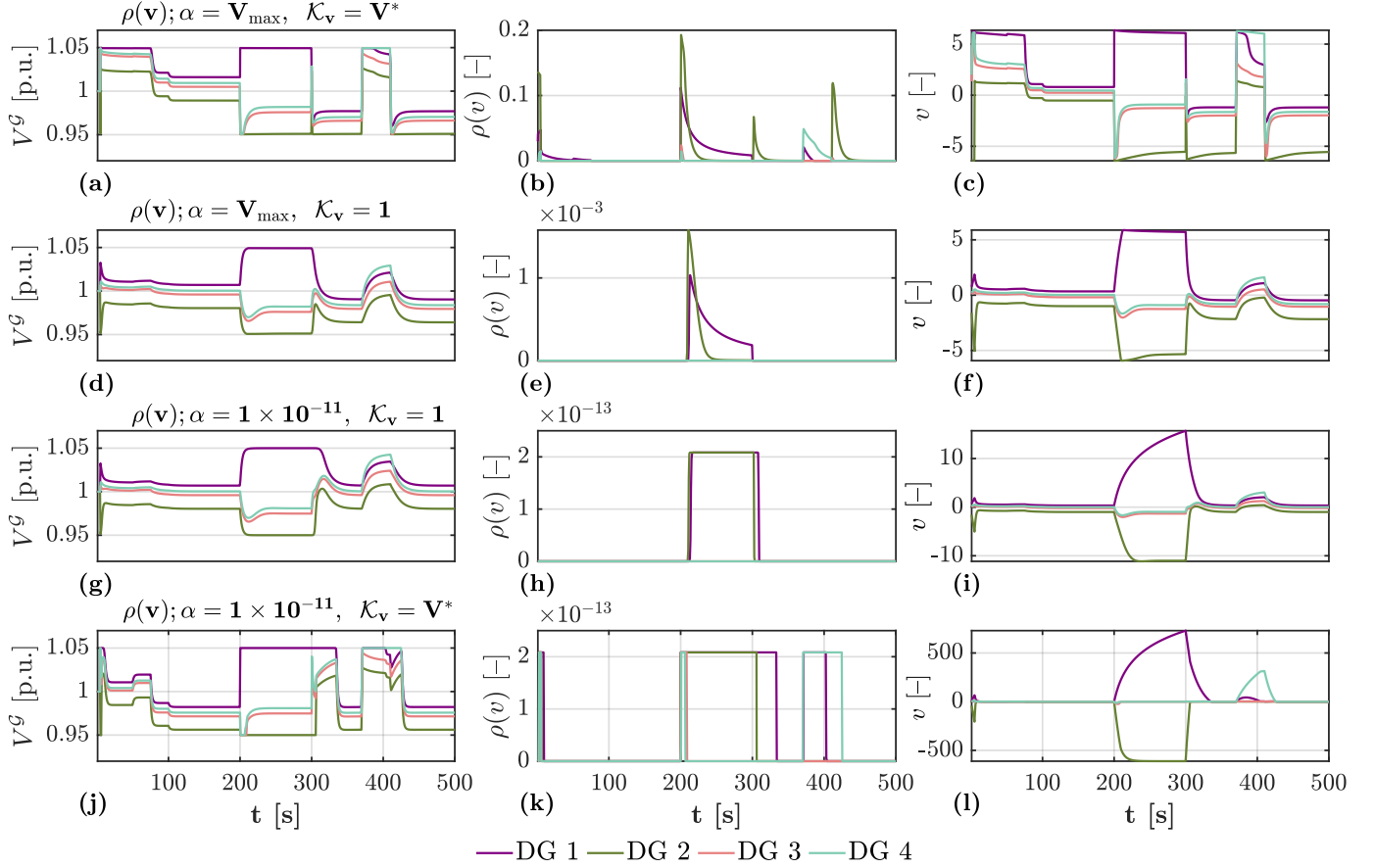
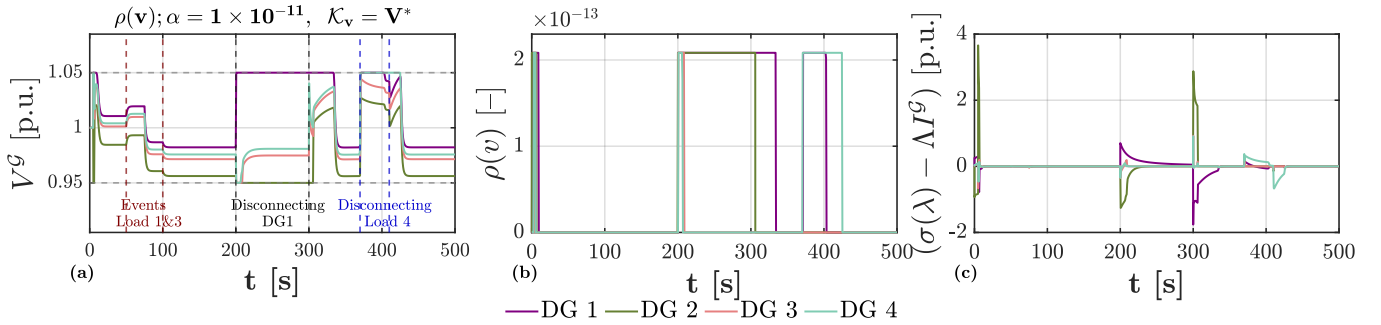
Fig. 4: System Response for varying values of  $\alpha$  and  $K_v$ ; (a), (d), (g), and (j) generator voltages; (b), (e), (h), and (k) leakage function; (c), (f), (i), and (l) controller state values

Fig. 5: System performance: (a) generator voltages; (b) leakage function; (c) integration errors



the decentralized controller states,  $v$ , beyond saturation limits, as seen in Fig. 4 (c) versus Fig. 4 (f). This leads to faster voltage saturation in the DG voltages (Fig. 4 (a) versus Fig. 4 (d)) and more frequent leakage ( $\rho(v)$ ) activation with elevated values, as shown in Fig. 4 (b) compared to Fig. 4 (e). However, when comparing Fig. 4(a) and Fig. 4 (d), it is evident that higher  $\mathcal{K}_v$  improves the convergence rate. Moreover, increasing  $\mathcal{K}_v$  enhances the dynamic response rate of the decentralized controller, as indicated by a reduction in the associated time constant ( $\tau/\mathcal{K}_v$ ). Moreover, this further amplifies the time-scale separation, thereby improving the large-signal stability conditions. In the third and fourth rows in Fig. 4, we impose a negligible leakage value ( $\alpha = 1 \times 10^{-11}$ ) to satisfy *Corollary 1* as per Section IV-A. When comparing Fig. 4 (f) and Fig. 4 (i), it is evident that minimizing the leakage pushes the  $v$ -values further beyond the values of saturation, as the inactive leakage function allows integrators to overshoot; i.e., it keeps integrating the control states. Moreover, lower  $\mathcal{K}_v$  and slow outer loop dynamics delay restoration to optimal steady state, as visualized in 4 (g) compared to Fig. 4 (j). Consequently, a higher  $\mathcal{K}_v$  improves this, as seen in faster stabilization of the DG voltages.

To summarize, increasing the leakage function enhances the control framework performance, aligning system operation more closely with the optimal steady state. However, this introduces dependencies within the electrical system. To ensure large-signal stability – approximating the inter-dependencies to zero – we reduce the value of  $\alpha$  and compensate by increasing  $\mathcal{K}_v$ , accelerating the rate of convergence. The system response is shown in Fig. 5, where Fig. 5 (c) illustrates the integration error. For *optimal* proportional current sharing, this error should ideally consistently be zero. As the rate of convergence increases, we observe that although the integration error exhibits spikes, it converges to zero in steady state, ensuring optimal current sharing.

### C. Case Study: Small-Signal Stability Analysis

We conducted a small-signal stability analysis to explore less conservative stability bounds, broadening the applicability of our results. Given that large-signal stability is preserved within substantial margins – characterized by significant time-scale separation between the nested control loops – we explore the possibility of operating the system under reduced *large-signal* stability margins for slower communication rates. To assess the impact of increased communication rates, we plot the eigenvalues of the DC MG for a parametric sweep of communication time constants  $\tau_p, \tau_d$  in Fig. 6 (a)(b). Additionally, we analyze the eigenvalues for varying values of the leakage coefficient  $\alpha$  in Fig. 6 (c). The distributed controller, reliant on cyber-network topologies defined by the Laplacian matrix, yields one near-zero eigenvalue. To enhance small-signal stability, we have included a constant leakage ( $\mathcal{B}_v$ ) in (4d), which combined with the negligible  $\mathcal{B}_\zeta$  (implemented in (4f) to compensate for the lack of structure in Section III-B), shifts the eigenvalues close to zero further into the left-half plane while maintaining optimal equilibrium ( $\lambda_i = \lambda_j$  and  $\zeta \approx 0$ ) when tuned as follows;  $\mathcal{B}_v = 1 \times 10^{-5}$ , and  $\mathcal{B}_\zeta = 1 \times 10^{-3}$  – as detailed in Table II.

TABLE II: Equilibrium when  $\mathcal{B}_\zeta = 1 \times 10^{-3}$  and  $\mathcal{B}_v = 1 \times 10^{-5}$

$\lambda_1$	$\lambda_2$	$\lambda_3$	$\lambda_4$	$\zeta_1$	$\zeta_2$	$\zeta_3$	$\zeta_4$
-0.3100	-0.3100	-0.3100	-0.3100	0.00	0.00	0.00	0.00

Fig. 6 (a)(b) shows that increasing communication rates from 100 times slower to 100 times faster than the electrical system moves the eigenvalues toward positive real values, approaching instability,

though the system remains stable for all  $\tau_p, \tau_d$ . Moreover, the parametric sweep of  $\alpha$  in Fig. 6(c) reveals that the leakage function  $\rho(v)$  has negligible impact on small-signal stability, as it is inactive at the converged equilibrium where voltages consistently stay within saturation limits; i.e., the eigenvalues are kept constant during this sweep.

This reinforces the strength of the large-signal stability analysis, despite its conservative time-scale constraints. The small-signal analysis alone might misleadingly suggest instability as eigenvalues approach zero, but the large-signal analysis confirms global stability and provides tuning insight. Moreover, from a practical viewpoint, the system remains stable under small-signal disturbances, even with faster communication rates, though with reduced stability margins. Thus, faster communication may allow for increased area of application, but requires practitioners to rely more on additional studies to compensate for the lack of large-signal stability guarantees, though, e.g., numerical/simulation-based analysis or time-domain simulations, which are more resource-intensive, time-consuming, case-specific, or require linearization.

### D. Case Study: PI Controller

Finally, we incorporate the widely used proportional-integral controller. The theoretical stability analysis in Section III accounts for this proportional component, however, previous simulation results were obtained assuming that the proportional gain  $\mathcal{K}_P$  was zero. In this case study, we investigate the control performance with a non-zero proportional gain, specifically setting  $\mathcal{K}_P = 10$ . Accordingly, the actuator weightings are updated to reflect the influence of the voltage containment function  $\Omega_1$  and the proportional controller  $\Omega_2$ . We assign  $\Delta_1$  to participate with 70% of  $\Delta$  and  $\Delta_2$  30%, where  $\Delta$  denotes the allowable voltage deviation range. In the previous case study (Section IV-B), Fig. 5(c) illustrates that transient and sharp current peaks emerge in the integration error. However, with the proportional controller activated – contributing 30% to the overall voltage containment – the system response shown in Fig. 7(b) demonstrates a significant reduction in these current peaks. Moreover, Fig. 7(c) presents the system behavior without the proportional controller, but with reduced decentralized control activity, contributing only 70% to the voltage containment. While this adjustment alone does reduce the current peaks compared to the response in Fig. 5(c), the combined implementation of the proportional controller and tuning yields a more substantial suppression of these peaks. Moreover, the simulations in Fig. 5(a) confirm that the introduction of the PI controller maintains overall system stability and ensures voltage containment within the predefined operational bounds.

## V. CONCLUSION AND FUTURE WORK

This paper obtained a global exponential stability (G.E.S) certificate for a *scalable* distributed nonlinear control framework in DC microgrids, altering the model presented in [1]. Our control modifications facilitate applying *singular perturbation theory* to prove G.E.S., by imposing a sufficient time-scale separation at the border between the decentralized inner loop and distributed outer loop controllers, preserving the mathematical structure of both separated systems when we saturate the influence of the slow dynamics in the fast dynamics. Our stability result requires careful tuning of the leakage function to reduce interdependencies in the electrical system. Time-domain simulations of a case-specific MG admitting the studied dynamics validate the effectiveness of the proposed method. From a performance

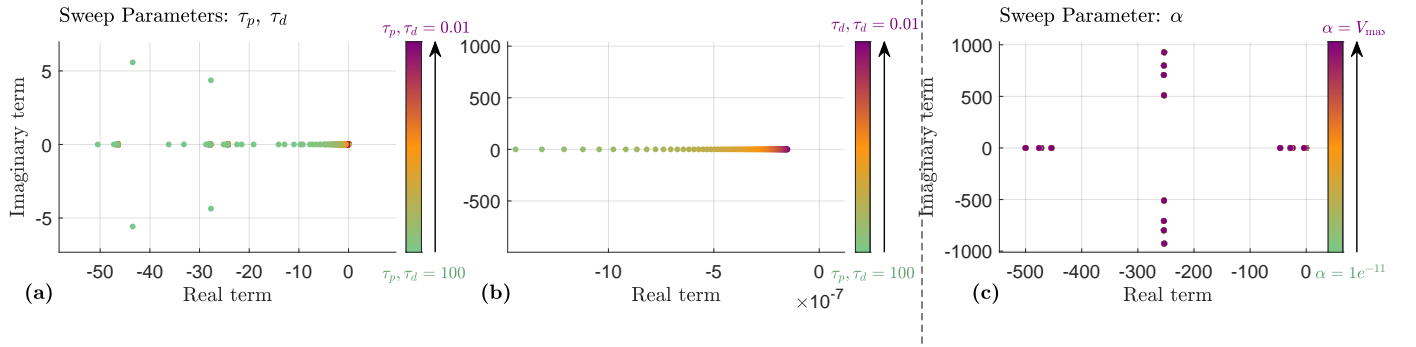


Fig. 6: Eigenvalues; (a) and (b) eigenvalues for a parametric sweep of  $\tau_p, \tau_d$ , (b) detailed image around zero; (c) eigenvalues for a parametric sweep of  $\alpha$

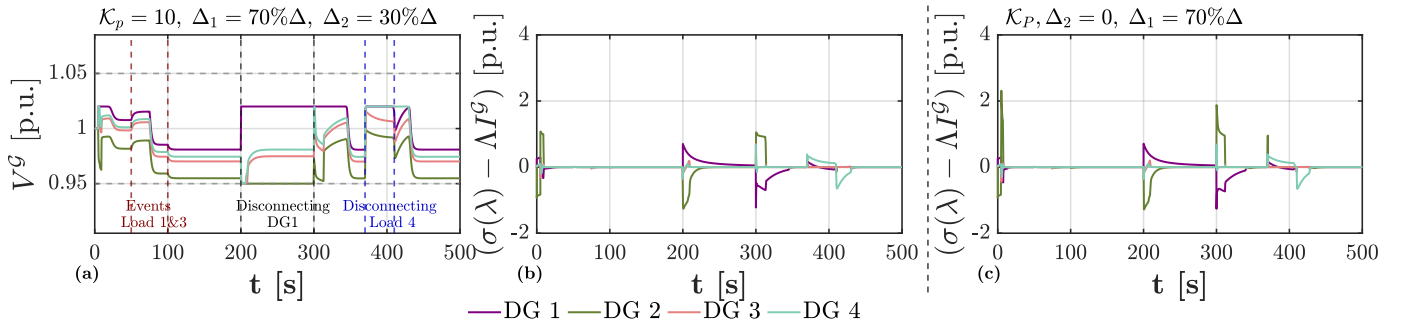


Fig. 7: System performance under PI control; (a) generator voltages; (b) integration error; (c) integration error with weighted integral controller (no proportional controller)

perspective, the simulations illustrate that under a small enough tuning value of the leakage function, combined with careful tuning of the integral gain, the system converges to optimal steady-state operations, achieving proportional current sharing while consistently maintaining voltages within permissible limits. Furthermore, implementing the PI-controller and limiting the range of the decentralized controller substantially improves the control performance by reducing unwanted current peaks. It is worth noting that the weighting scheme of the PI controller presents opportunities for further optimization. Specifically, a logical switching mechanism that dynamically adjusts the contributions of the individual saturation functions. Such adaptive tuning may enhance control robustness, performance, and effective current peak shaving under varying operational conditions. Additionally, future work may explore the possibility of saturating the PI controller as a whole. However, such an approach would introduce additional complexity, particularly when applying singular perturbation theory. Moreover, the large-signal stability certificate ensures *scalable* stability with robust margins, characterized by significant time-scale separation. To complement our large-signal control design, we performed a small-signal stability analysis, which resulted in practical guidelines to expand the applicability for a less conservative time-scale separation. Indeed, operating outside the large-signal tuning conditions can still be compensated by performing additional studies; e.g., more time-domain simulations or eigenvalue analysis.

## REFERENCES

- [1] C. Skaga and G. Bergna-Diaz, "A distributed control framework with scalable stability guarantees for dc current sharing under voltage limits," *IEEE SEST*, 2024.
- [2] B. Abdolmaleki, J. Simpson-Porco, and G. Bergna-Diaz, "Distributed optimization for reactive power sharing and stability of inverter-based resources under voltage limits," *IEEE Transactions on Smart Grid*, vol. 15, no. 2, pp. 1289–1303, 2024.
- [3] S. Sahoo, J. Chih-Hsien, A. Devakumar, S. Mishra, and T. Dragičević, "On detection of false data in cooperative dc microgrids—a discordant element approach," *IEEE Transactions on Industrial Electronics*, vol. 67, no. 8, pp. 6562–6571, 2020.
- [4] B. Abdolmaleki and G. Bergna-Diaz, "A nonlinear control framework for optimal load-sharing and voltage containment in dc networks," *IEEE Transactions on Power Systems*, vol. 38, no. 1, pp. 976–979, 2023.
- [5] X. Huo, H. Huang, K. R. Davis, H. V. Poor, and M. Liu, "A review of scalable and privacy-preserving multi-agent frameworks for distributed energy resources," *Advances in Applied Energy*, vol. 17, p. 100205, 2025.
- [6] S. Sahoo, T. Dragičević, and F. Blaabjerg, "An event-driven resilient control strategy for dc microgrids," *IEEE Transactions on Power Electronics*, vol. 35, no. 12, pp. 13 714–13 724, 2020.
- [7] A. Cecilia, S. Sahoo, T. Dragičević, R. Costa-Castelló, and F. Blaabjerg, "Detection and mitigation of false data in cooperative dc microgrids with unknown constant power loads," *IEEE Transactions on Power Electronics*, vol. 36, no. 8, pp. 9565–9577, 2021.
- [8] B. Abdolmaleki and G. Bergna-Diaz, "Distributed control and optimization of dc microgrids: A port-hamiltonian approach," *IEEE Access*, vol. 10, pp. 64 222–64 233, June 2022.
- [9] D. Ferreira, S. Silva, W. Silva, D. Brandao, G. Bergna-Diaz, and E. Tedeschi, "Overview of consensus protocol and its application to microgrid control," *Energies*, 2022.
- [10] E. Espina, J. Llanos, C. Burgos-Mellado, R. Cárdenas-Dobson, M. Martínez-Gómez, and D. Sáez, "Distributed control strategies for microgrids: An overview," *IEEE Access*, vol. 8, pp. 193 412–193 448, 2020.
- [11] T. Dragičević, X. Lu, J. C. Vazquez, and J. M. Guerrero, "Dc microgrids—part i: A review of control strategies and stabilization techniques," *IEEE Transactions on Power Electronics*, vol. 31, no. 7, pp. 4876–4891, 2016.
- [12] A. Wang, M. Fei, and Y. Song, "A novel scalable and reliable control for dc microgrids with varying number of agents," *IEEE Transactions on Cybernetics*, vol. 3, no. 3, pp. 1–11, 2024.
- [13] L. Xiong, X. Liu, Y. Liu, and F. Zhuo, "Modeling and stability issues of voltage-source converter-dominated power systems: A review," *CSEE Journal of Power and Energy Systems*, vol. 8, no. 6, pp. 1530–1549, 2022.
- [14] D. Pullaguram and S. Sahoo, "Cyber security in multi-agent microgrids," in *Cyber Security for Microgrids*, D. Pullaguram and S. Subham, Eds. Stevenage: The Institution of Engineering and Technology, 2022, pp. 105–125.

- [15] M. Cucuzzella, S. Trip, C. D. Persis, X. Cheng, A. Ferrara, and A. van der Schaft, "A robust consensus algorithm for current sharing and voltage regulation in dc microgrids," *IEEE Transaction on Control System Technology*, vol. 27, no. 4, pp. 1583–1595, 2019.
- [16] —, "A robust consensus algorithm for current sharing and voltage regulation in dc microgrids," *IEEE Transactions on Control Systems Technology*, vol. 27, no. 4, pp. 1583–1595, 2019.
- [17] S. Trip, M. Cucuzzella, X. Cheng, and J. Scherpen, "Distributed averaging control for voltage regulation and current sharing in dc microgrids," *IEEE Control Systems Letters*, vol. 3, no. 1, pp. 174–179, 2019.
- [18] J. Zhao and F. Dörfler, "Distributed control and optimization in dc microgrids," *Automatica*, vol. 61, pp. 18–26, 2015.
- [19] C. D. Persis, E. Weitenberg, and F. Dörfler, "A power consensus algorithm for dc microgrids," *Automatica*, vol. 89, pp. 364–375, 2018.
- [20] V. Nasirian, S. M. A. Davoudi, and F. Lewis, "Distributed cooperative control of dc microgrids," *IEEE Transactions on Power Electronics*, vol. 30, no. 4, pp. 2288–2303, 2015.
- [21] S. Sahoo, D. Pullaguram, S. Mishra, J. Wu, and N. Senroy, "A containment based distributed finite-time controller for bounded voltage regulation & proportionate current sharing in dc microgrids," *Applied Energy*, vol. 228, pp. 2526–2538, 2018.
- [22] V. Nasirian, S. Moayedi, A. Davoudi, and F. Lewis, "Distributed cooperative control of dc microgrids," *IEEE Transactions on Power Electronics*, vol. 30, no. 4, pp. 2288–2303, 2015.
- [23] B. Fan, S. Guo, J. Peng, Q. Yang, W. Liu, and L. Liu, "A consensus-based algorithm for power sharing and voltage regulation in dc microgrids," *IEEE Transactions on Industrial Informatics*, vol. 16, no. 6, pp. 3987–3996, 2020.
- [24] M. Cucuzzella, S. Trip, C. D. Persis, X. Cheng, A. Ferrara, and A. van der Schaft, "A robust consensus algorithm for current sharing and voltage regulation in dc microgrids," *IEEE Transactions on Control System Technology*, vol. 27, no. 4, pp. 1583–1595, 2019.
- [25] N. Monshizadeh, F. Mancilla-David, R. Ortega, and R. Cisneros, "Nonlinear stability analysis of the classical nested pi control of voltage sourced inverters," *IEEE Control System Letters*, vol. 6, pp. 1442–1447, 2020.
- [26] C. Skaga, B. Abdolmaleki, and G. Bergna-Diaz, "Stability of a distributed controller for optimal current sharing and voltage containment in dc microgrids," *IEEE GPECOM*, 2024.
- [27] H. K. Khalil, *Nonlinear systems*, 3rd ed. Prentice Hall, 2002.